P11 Utilizing Ensemble Sensitivity for Data Denial Experiments of the 4 April 2012 Dallas, Texas Dryline-Initiated Convective Outbreak Using West Texas Mesonet Observations and WRF-DART Data Assimilation

Aaron J. Hill*, Christopher C. Weiss, and Brian C. Ancell
Texas Tech University, Lubbock, Texas

1. Introduction

Ensemble-based sensitivity analysis (ESA) details how changes in initial condition errors affect a chosen scalar forecast metric by utilizing background and forecast error from an ensemble sample of forecasts. ESA implies a linear change of a forecast metric due to changes in the initial conditions and can be used to further understand the dynamic evolution of errors. Ensemble sensitivity was first introduced by Hakim and Torn (2008), followed by Ancell and Hakim (2007) and Torn and Hakim (2008), as a means to examine the linear relationship between forecast surface pressure of an extra-tropical cyclone making landfall over Western Washington and initial conditions over the Pacific ocean. Further studies have examined the usefulness of ESA towards extra-tropical cyclones (Garcies and Homar 2009, 2010; Chang et al. 2013), tropical cyclones (Xie et al. 2013), extra-tropical transition (Torn and Hakim 2009), African easterly waves (Torn 2010), and mesoscale wind generation from synoptic scale interactions (Zack et al. 2010).

Development of ESA applications were explored by Ancell and Hakim (2007), utilizing ESA and the ensemble Kalman filter (EnKF; Evensen 1994) to target locations where the atmosphere could be observed to reduce forecast uncertainty. Various targeting techniques have been employed to adaptively observe synoptic scale features, including the ensemble transform technique (Szunyogh et al. 2000), ensemble transform Kalman filter (ETKF; (Szunyogh et al. 1999; Bishop et al. 2001; Hamill et al. 2013), conditional nonlinear optimal perturbations (Qin and Mu 2011), and adjoint methods (Langland and Baker 2004). Hamill and Snyder (2002) targeted observations to reduce analysis-error variance in hopes of reducing error at a forecast lead time which showed to be successful for some assimilation schemes but not others. Targeting techniques outlined by Ancell and Hakim (2007) require only a sample of ensemble members from an EnKF data assimilation procedure integrated forward with an atmospheric model. By calculating sensitivity and targeted regions based solely on sample statistics, ESA targeting becomes a much simpler formula than other targeting techniques mentioned previously.

The goal of this study is to perform data denial experiments and perform ESA to determine if observation targeting for convective forecasts is feasible given the non-linear and binary nature of convective initiation (CI) and evolution within an

*Corresponding author address: Aaron J. Hill, Texas Tech University, Atmospheric Science Group, Department of Geosciences, Lubbock, TX, 79409; e-mail: aaron.hill@ttu.edu

ensemble of forecasts. Given that the expected change in forecast metric variance can be estimated, it is also possible to analyze if predictions of variance reduction correlate with the actual change in forecast uncertainty (variance and uncertainty are used interchangeably throughout this study). Future plans include applying adaptive observation targeting into a real-time ensemble forecasting system in use at Texas Tech University. With adaptive observing platforms available, in situ observations can be gathered at targeted locations in real-time and assimilated into the data assimilation scheme for subsequent real-time forecasts with reduced forecast uncertainty.

2. Experimental Setup

A 50-member ensemble of analyses is chosen from an ensemble adjusted Kalman filter (Anderson 2001) that utilizes the Weather Research and Forecasting (WRF) model v3.3. Three one-way nested domains are implemented at 36km, 12km and 4km grid spacing (Figure 1) with 38 vertical levels. The Data Assimilation Research Testbed (DART; Anderson et al. 2009) is employed to combine observations with the model state. Covariance localization (Anderson 2001) is used to reduce the effects of spurious covariance at a large distance from the observation. The Gaspari-Cohn localization function (Gaspari and Cohn 1999) is chosen with a half-width of ~300km so that the observation's influence is one at the observation location and zero at a distance two times the half-width following a Gaussian weighting function. Spatially and temporally adapting covariance inflation (Anderson 2009) is utilized to increase ensemble variance, accounting for model and observational error that may create an under dispersive ensemble and subsequent filter divergence. A 6-hour update cycle is performed for 24 hours from 0000 UTC 2 April 2012 to 0000 UTC 3 April 2012 on all domains using observations from land-based surface stations, radiosonde networks, buoys, ships, and aircraft measurements shown in Table 1. Doman one (36km) is cycled for 24 hours prior to the innermost domains to develop flow dependence.

All 50 members are advanced 24 hours from 0000 UTC 3 April 2012 to 0000 UTC 4 April 2012 with lateral boundary conditions for the outermost domain obtained from the Global Forecast System (GFS) forecasts. Boundary conditions for the nested domains are obtained from their respective parent domain. Various parameterization schemes are utilized to account for sub-grid scale phenomena, including Thompson microphysics, Rapid Radiative Transfer Model (RRTM) longwave radiation, Dudhia shortwave radiation, Kain Fritsch cumulus, Noah land surface, and Yonsei boundary layer schemes. To more appropriately represent convection on the innermost domain, no cumulus parameterization scheme is used.

2.1 Sensitivity and Targeting

Sensitivity is calculated as the linear regression of a forecast metric (J) to initial condition variable (x) (Figure 2). This is mathematically equivalent to,

$$\frac{\partial J}{\partial x} = \frac{covar(J,x)}{var(x)} \quad (1)$$

The quotient of the covariance between J and x and variance in the initial conditions represents how J will change with an incremental change in x. A full derivation for (1) can be found from Ancell and Hakim (2007). Targeting locations are found through a similar derivation that is mathematically equivalent to Ancell and Hakim (2007) equation 22,

$$\delta\sigma = \frac{covar^2(J,x)}{var(x)+var(ob)} \quad (2)$$

where σ represents the forecast metric variance and var(ob) is the observation error variance. Targeting values at different locations reveal that if observations were taken and assimilated into the data assimilation system, they would reduce the forecast variance by an expected amount from (2). Such a value would be easily computed with dependence only on the ensemble statistics between J and x and an assumed observational error, obtained from instrumentation directly.

In order to correctly target a convective forecast, forecast parameters that are relevant to convection must be chosen. For our study, chosen forecast metrics included maximum reflectivity, maximum vertical velocity, and average 2-meter temperature as defined within the 64x120 km black rectangle as seen in Figure 4. Maximum reflectivity and vertical velocity were chosen for their representation of large hydrometeors and strong updrafts, consistent with vigorous convection. Average 2-meter temperature was chosen as a benchmark variable, representing a more linear relationship between the initial condition and forecast compared to reflectivity or vertical velocity. It should be noted, however, that 2-meter temperature also exhibits non-linearity to a chosen initial condition with the formation of cold pools from convective storms. For simplicity, only 2-meter temperature is used as the initial condition variable, although it should be understood any state variable may be used.

2.2 Data Denial Experiments

In order to determine where additional observations will have the greatest impact on forecast uncertainty, a series of data denial experiments are set up to accurately choose West Texas Mesonet (WTM) stations that will most influence the chosen forecast metric. Assessments of expected versus actual variance reduction are completed by withholding observations from the West Texas Mesonet (WTM, Figure 3) in the general set of assimilated observations. A control run is performed via the data assimilation methods detailed previously and performing a 24 hour forecast initialized at 0000 UTC 3 April 2012, integrating all ensemble members forward. Ensemble sensitivity and targeting fields are then calculated across the domain. The WTM station that exhibits the highest expected forecast metric variance reduction (targeting value) is chosen as the location to assimilate observations. The 2-meter temperature at the station is assimilated at initialization and a subsequent ensemble forecast is produced. Targeting is calculated again for the new ensemble forecast. This procedure is repeated for five stations and each forecast metric. The expected variance after each new assimilated observation is the sum of expected variance reduction for all previous stations subtracted from the control simulation variance.

3. Case Overview

On 3 April 2012, convection west of the Dallas/Fort. Worth metroplex in North Texas initiated a number of discrete supercells that produced 22 tornadoes, as reported by the Storm Prediction Center (http://www.spc.noaa.gov/climo/reports/120403_rpts.html). Early afternoon convection in Central Oklahoma forced an outflow boundary southward during the early afternoon as a dryline propagated eastward through Central Texas. Mean composite reflectivity and maximum vertical velocity at 00 UTC on 4 April show the north-south oriented convection in Oklahoma with the largest spread in the reflectivity field toward the southern periphery in North Texas, indicative of some ensemble members producing CI and others not (Figure 4 a, b). The two boundaries collided in north-central Texas and initiated convection at approximately 1900 UTC 3 April 2012. The 2-meter temperature mean and spread fields in Figure 4 (c) further illustrates the uncertainty in the ensemble and where convection will occur in North Texas. The ensemble missed on the timing and placement of convection, an ideal forecast to improve through targeted observations.

4. Results

Sensitivity fields reveal features in the initial conditions that are related to the chosen forecast metric. Further examination is needed to understand whether these features are dynamically linked (e.g. the driving upper-level trough), or whether they are simply statistically related (e.g. a downstream ridge). Figure 5 shows the sensitivity fields for the three forecast metrics chosen, maximum reflectivity, maximum vertical velocity, and average 2-meter temperature. Sensitivity of reflectivity and vertical velocity at forecast hour 24 to 2-meter temperature at forecast initialization (Figure 5 a, b) is maximized in the southeast corner of the domain over the Gulf of Mexico, where an incremental increase of 2-meter temperature at hour zero is associated with an increase in maximum reflectivity and maximum vertical velocity at hour 24. This could represent a dynamical relationship of advected warm air from the Gulf of Mexico influencing convection by increasing surface temperature and dewpoints, subsequently enhancing convection. A local minimum in the sensitivity field also exists for reflectivity and velocity in eastern New Mexico where an increase in 2-meter temperature would be associated with a decrease in the forecast metric. This signature may indicate that a warmer surface environment over New Mexico and West Texas could inhibit convection over Central Texas 24 hours later. Because West Texas is elevated from the Central Texas land height, warmer air advected eastward may act as a capping inversion at upper levels, effectively limiting convective development. Furthermore, a negative sensitivity in Central Oklahoma may be related to air advected via the outflow boundary into central Texas. A warmer environment in Oklahoma 24 hours prior to CI would inhibit convective development according to this sensitivity signature. Various local minima and maxima throughout the domain are most likely due to spurious covariance relationships between J and x and a more robust experiment with multiple similar cases could remove such sensitivity

values. The average 2-meter temperature forecast metric is harder to analyze with various positive and negative sensitivity dispersed somewhat randomly throughout the domain (Figure 5 c). Some of the largest sensitivity values are located along a north-south oriented line, parallel to the forecast metric region, which may indicate the importance of day previous surface temperatures to convection.

Targeting fields illustrate a vastly different picture than sensitivity, noting that targeted locations exist primarily along a north-south line over Central West Texas that is collocated with the position of a dryline at forecast initialization which are located away from regions of largest sensitivity (Figure 6). The difference in targeting and sensitivity fields is due to the inclusion of an additional covariance term in (2), highlighting the relationship of forecast metric to initial conditions in reducing forecast metric variance. These targeted locations suggest that if the atmosphere is observed 24 hours prior to CI, and those observations are assimilated into the forecast model, forecast metric uncertainty will decrease by an expected amount consistent with the calculations performed. Given the similarities of target regions for all metrics, this suggests the importance of day prior dryline positioning for convective initiation, which is reasonable given the dryline and outflow-driven convection.

To select targeted observations, WTM stations were chosen based on targeting fields and maximizing forecast uncertainty reduction. The chosen stations are not discussed further but the majority existed on the eastern periphery of the WTM array. Results of expected versus actual variance reduction can be seen in Figure 7 with expected and actual variance displayed in red and blue, respectively. For each forecast metric, actual variance changes did not match the expected variance reduction of the forecast metric. In some cases, additional observations increased the forecast metric variance which does not match targeting theory; variance reduction is positive definite (Ancell and Hakim 2007; Torn and Hakim 2008). For all observations assimilated, only average temperature experienced an overall reduction in variance. Maximum reflectivity and vertical velocity saw a slight increase in variance with the addition of five observations. However, both localization and inflation can act to alter the actual variance reduction, which is not quantified and accounted for in this study. In addition, various assumptions are made in ESA and observation-targeting theory that may not completely align with a convective case as has been presented. The forecast metric is assumed to have a Gaussian distribution amongst the ensemble members, which in this case is not true for either maximum reflectivity or vertical velocity (Figure 2 a, b). The scatters of maximum reflectivity and vertical velocity show a bimodal distribution of reflectivity and a lower-value weighted distribution of vertical velocity. Likewise, ESA and targeting are based off a linear relationship between the forecast metric and initial conditions. If the distribution of the metric is bimodal, a linear regression of the two variables will not correctly identify the true relationship. The non-linear nature of convection also plays a role in that a linear assumption may be insufficient to accurately target locations to reduce forecast uncertainty

that is strictly non-linear at 24-hour lead-time.

5. Conclusions and Future Work

This study examines the effectiveness of applying ensemble-based sensitivity analysis and observation targeting methodology on a mesoscale convective-initiation forecast to determine if forecast uncertainty can be reduced by assimilating additional observations into a forecast system and if reductions can be accurately predicted. Utilizing a WRF-EnKF DART modeling framework, a series of data denial cases were presented to assess observational impacts on forecast uncertainty. A control simulation was executed that assimilated a base set of observations, with ensemble sensitivity and targeting calculations performed on the control simulation forecasts. West Texas Mesonet stations were selected and subsequently assimilated that exhibited the largest degree of expected variance reduction of chosen scalar forecast metrics, maximum reflectivity, maximum vertical velocity, and average 2-meter temperature, within a rectangular region in the domain. A 2-meter temperature observation from the target WTM station was assimilated and a new simulation was performed. This process was repeated for five stations for each forecast metric. Generally, forecast expected variance reduction did not match the change in variance of the forecast metrics discovered. In some instances, additional observations increased the forecast uncertainty, which is not consistent with ESA and targeting theory. The five additional observations overall reduced the variance of average 2-meter temperature and slightly increased the maximum reflectivity and vertical velocity variance. Adaptations to the EnKF are made in the DART system, which could lead to alterations to the actual variance reduction from what is expected. In addition, linear relationship assumptions made in ESA may not hold true for a CI forecast. Additionally, the forecast metrics chosen may not have exhibited a Gaussian distribution, which is assumed in ESA. Future work will be completed to assess the impacts that these assumptions of linearity and Gaussian distributions, along with the localization and inflations features of DART, have on the actual variance reduction and if these factors can be predicted within the expected variance reduction calculations.

6. Acknowledgements

This study is funded by NOAA CSTAR grant NA11NWS4680001. The authors wish to thank Jeffery Anderson and Nancy Collins for their assistance with the DART system.

References

Ancell, B., and G. J. Hakim, 2007: Comparing adjoint- and ensemble-sensitivity analysis with applications to observation targeting. *Mon. Wea. Rev.*, **135**, 4117–4134.

Anderson, J., 2001: An ensemble adjustment kalman filter for data assimilation. *Mon. Wea. Rev.*, **129**, 2884–2903.

Anderson, J., T. Hoar, K. Raeder, H. Liu, N. Collins, R. Torn, and A. Avellano, 2009: The data assimilation research testbed: a community facility. *Bull. Amer. Meteor. Soc.*, **90**, 1283–1296.

Anderson, J. L., 2009: Spatially and temporally varying adaptive covariance inflation for ensemble filters. *Tellus A*, **61**, 72–83.

Bishop, C., B. J. Etherton, and S. J. Majumdar, 2001: Adaptive sampling with the ensemble transform kalman filter. part i: theoretical aspects. *Mon. Wea. Rev.*, **129**, 420–436.

Chang, E. K. M., M. Zheng, and K. Raeder, 2013: Medium-range ensemble sensitivity analysis of two extreme pacific extratropical cyclones. *Mon. Wea. Rev.*, **141**, 211–231.

Evensen, G., 1994: Sequential data assimilation with a nonlinear quasi-geostrophic model using monte carlo methods to forecast error statistics. *J. Geophys. Res.*, **99**, 10143–10162.

Garcies, L., and V. Homar, 2009: Ensemble sensitivities of the real atmosphere: application to mediterranean intense cyclones. *Tellus A*, **61**, 394–406.

Garcies, L., and V. Homar, 2010: An optimized ensemble sensitivity climatology of mediterranean intense cyclones. *Nat. Hazards Earth Sys. Sci.*, **10**, 2441–2450.

Gaspari, G., and S. Cohn, 1999: Construction of correlation functions in two and three dimensions. *Quart. J. Roy. Meteor. Soc.*, **125**, 723–757.

Hakim, G. J., and R. D. Torn, 2008: Ensemble synoptic analysis. *Synoptic-Dynamic Meteorology and Weather Analysis and Forecasting: A Tribute to Fred Sanders*, No. 55, Amer. Meteor. Soc., 147–161.

Hamill, T., and C. Snyder, 2002: Using improved background-error covariances from an ensemble kalman filter for adaptive observations. *Mon. Wea. Rev.*, **130**, 1552–1572.

Hamill, T. M., F. Yang, C. Cardinali, and S. J. Majumdar, 2013: Impact of targeted winter storm reconnaissance dropwindsonde data on midlatitude numerical weather predictions. *Mon. Wea. Rev.*, **141**, 2058–2065.

Langland, R. H., and N. L. Baker, 2004: Estimation of observation impact using the nrl atmospheric variational data assimilation adjoint system. *Tellus A*, **56**, 189–201.

Qin, X., and M. Mu, 2011: A study on the reduction of forecast error variance by three adaptive observation approaches for tropical cyclone prediction. *Mon. Wea. Rev.*, **139**, 2218–2232.

Szunyogh, I., Z. Toth, K. Emanuel, C. H. Bishop, C. Snyder, R. Morss, J. Woolen, and T. Marchok, 1999: Ensemble-based targeting experiments during fastex: the effect of dropsonde data from the lear jet. *Quart. J. Roy. Meteor. Soc.*, **125**, 3189–3217.

Szunyogh, I., Z. Toth, R. Morss, S. J. Majumdar, B. J. Etherton, and C. H. Bishop, 2000: The effect of targeted dropsonde observations during the 1999 winter storm reconnaissance

program. *Mon. Wea. Rev.*, **128**, 3520–3537.

Torn, R. D., 2010: Ensemble-based sensitivity analysis applied to african easterly waves. *Wea. Forecasting*, **25**, 61–78.

Torn, R. D., and G. J. Hakim, 2008: Ensemble-based sensitivity analysis. *Mon. Wea. Rev.*, **136**, 663–677.

Torn, R. D., and G. J. Hakim, 2009: Initial condition sensitivity of western pacific extratropical transitions determined using ensemble-based sensitivity analysis. *Mon. Wea. Rev.*, **137**, 3388–3406.

Xie, B., F. Zhang, Q. Zhang, J. Poterjoy, and Y. Weng, 2013: Observing strategy and observation targeting for tropical cyclones using ensemble-based sensitivity analysis and data assimilation. *Mon. Wea. Rev.*, **141**, 1437–1453.

Zack, J., E. Natenberg, and S. Young, 2010: Application of Ensemble Sensitivity Analysis to Observation Targeting for Short-term Wind Speed Forecasting. Technical Report LLNL-TR-424442, 32 pp., Lawrence Livermore National Laboratory, Livermore, CA.

	T	U wind	V wind	Q	RH	Td	Alt	P
Radiosonde	X	X	X	X	X	X	X (surf)	
Satellite		X	X					
ACARS	X	X	X	X	X	X		
METAR	X	X	X	X	X	X	X	X
Marine	X	X	X	X	X	X	X	
Land_Surface	X	X	X	X	X	X	X	
West Texas Mesonet	X							

Table 1: Observations used during the data assimilation cycle. Black X's mark observations that we always assimilated. Red X's represent observations that were altered for various simulations.

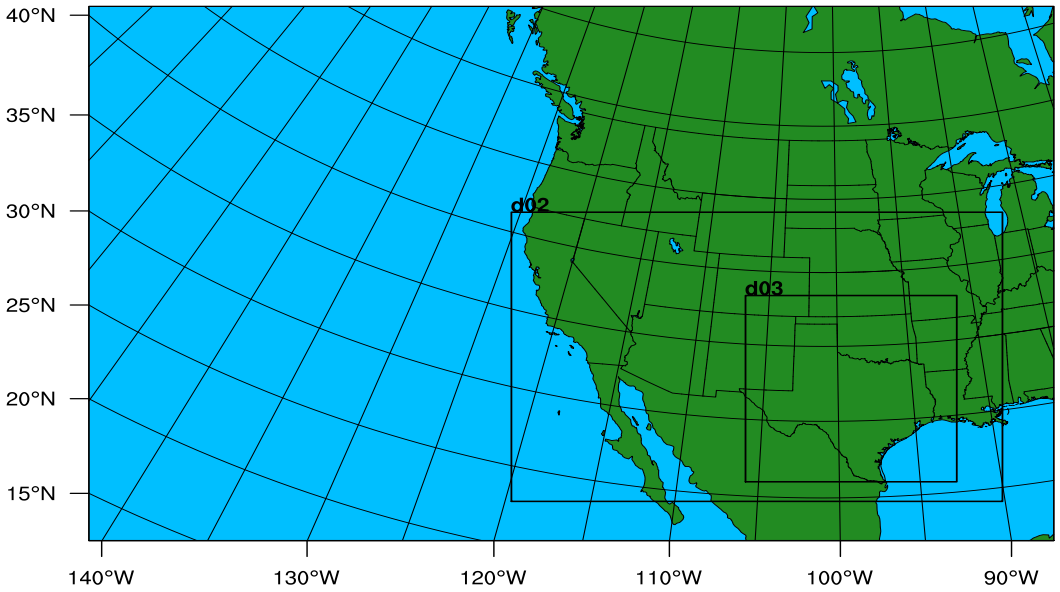

Figure 1: Three nested domains used during the study at 36km (d01), 12km (d02), and 4km (d03) grid spacing.

(a)

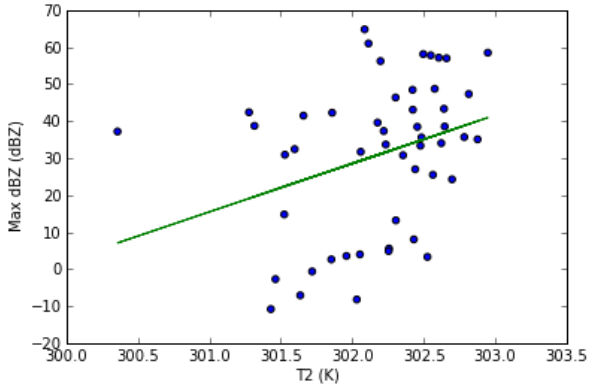

(b)

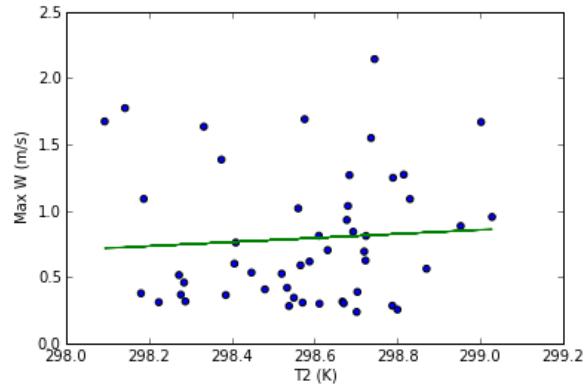

(c)

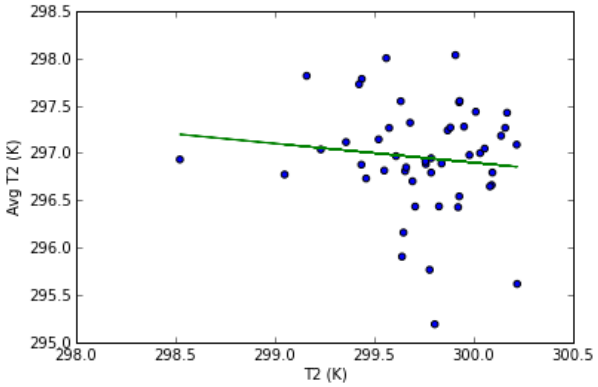

Figure 2: Scatters of forecast metrics (a) max dBZ (dBZ), (b) max vertical velocity (m s^{-1}), and (c) average 2-meter temperature (K) at forecast hour 24 against initial condition 2-meter temperature at model initialization. Lines indicate the linear regression between the two variables.

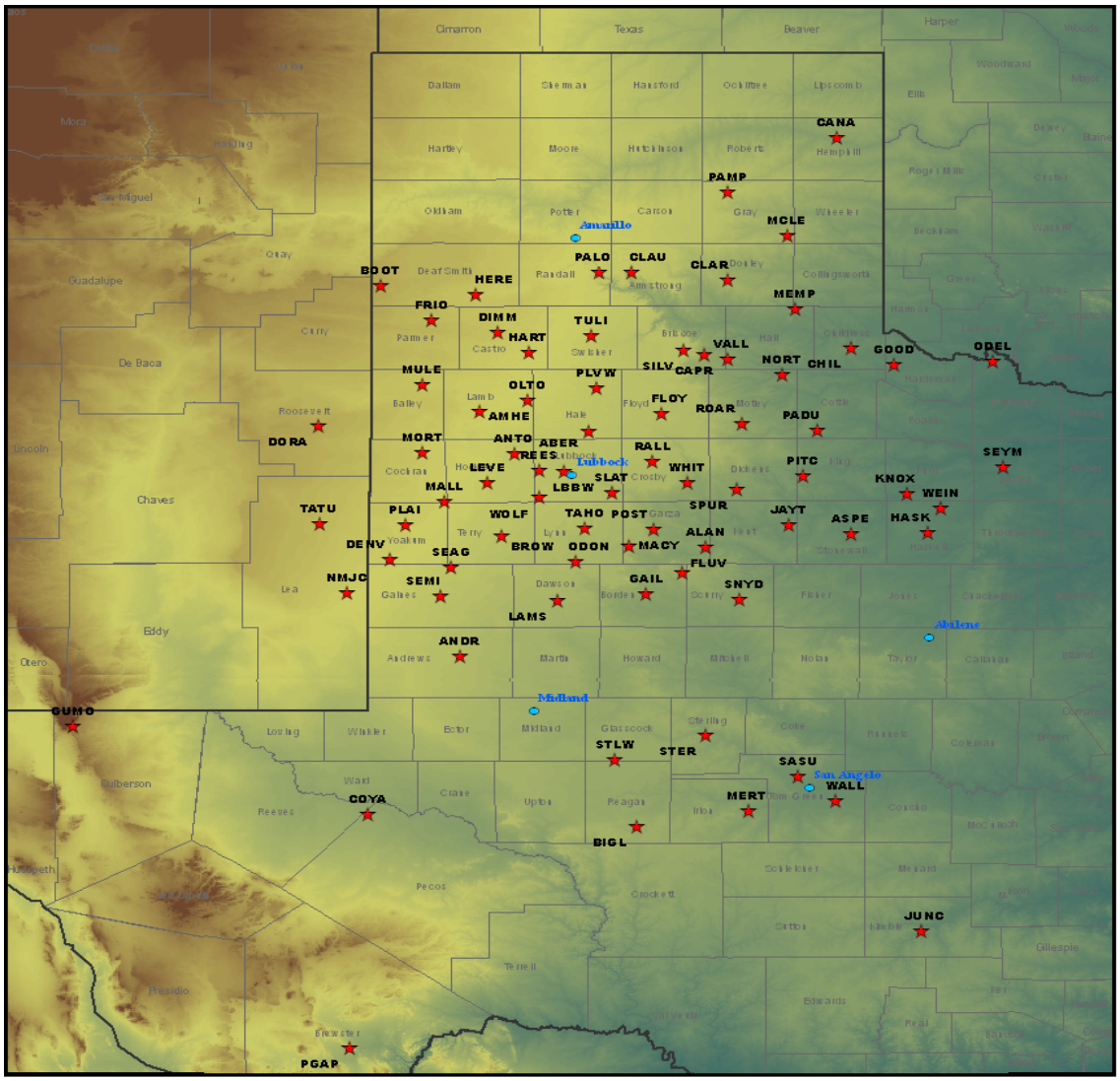

Figure 3: West Texas Mesonet array and four-letter station identifier.

(a)

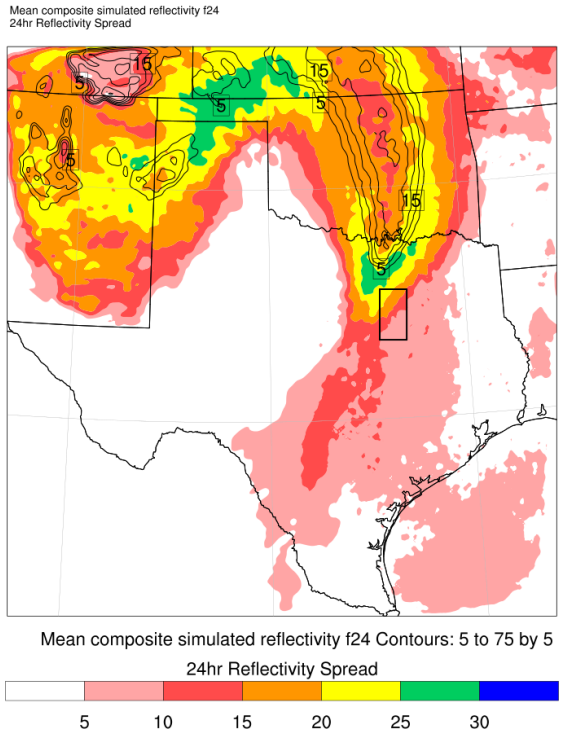
Mean composite simulated reflectivity f24
24hr Reflectivity Spread
15
5
15
5
5
15
5
Mean composite simulated reflectivity f24 Contours: 5 to 75 by 5
24hr Reflectivity Spread
5
10
15
20
25
30

(b)

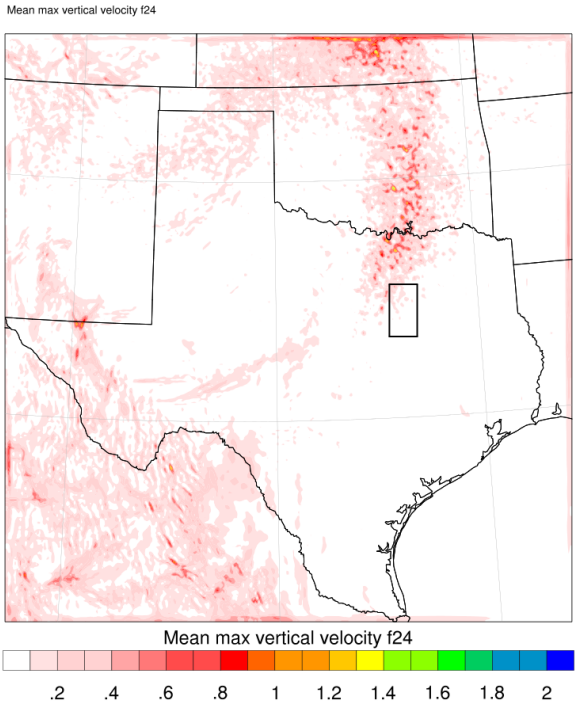
Mean max vertical velocity f24
Mean max vertical velocity f24
.2
.4
.6
.8
1
1.2
1.4
1.6
1.8
2

(c)

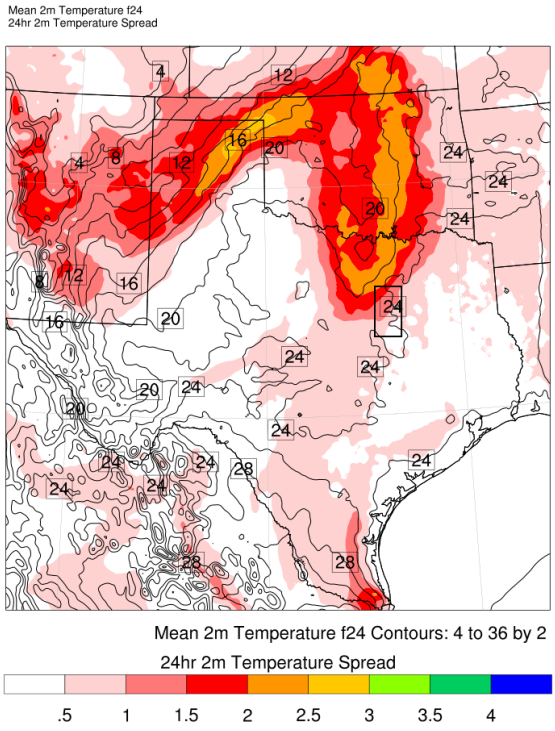

Figure 4: Ensemble mean of forecast metrics (a) max dBZ (contours, dBZ), (b) max vertical velocty (colored, m s^{-1}), and (c) average 2-meter temperature (contours, K). Ensemble spread of max dBZ and average 2-meter temperature are colored in (a) and (c). Forecast metric region shown with rectangular box.

(a)

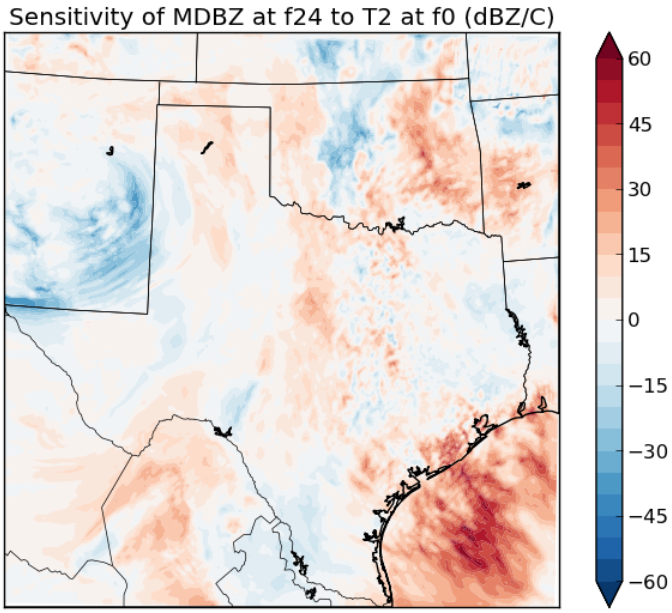
Sensitivity of MDBZ at f24 to T2 at f0 (dBZ/C)
60
45
30
15
0
−15
−30
−45
−60

(b)

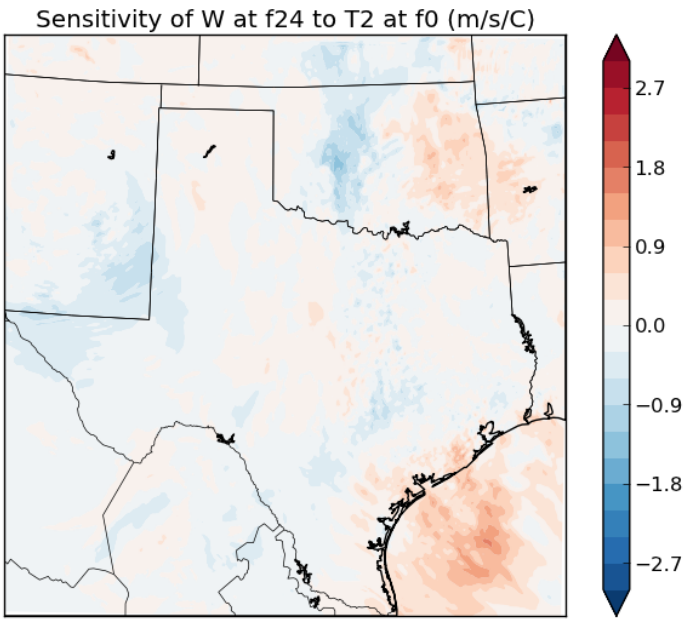
Sensitivity of W at f24 to T2 at f0 (m/s/C)
2.7
1.8
0.9
0.0
−0.9
−1.8
−2.7

(c)

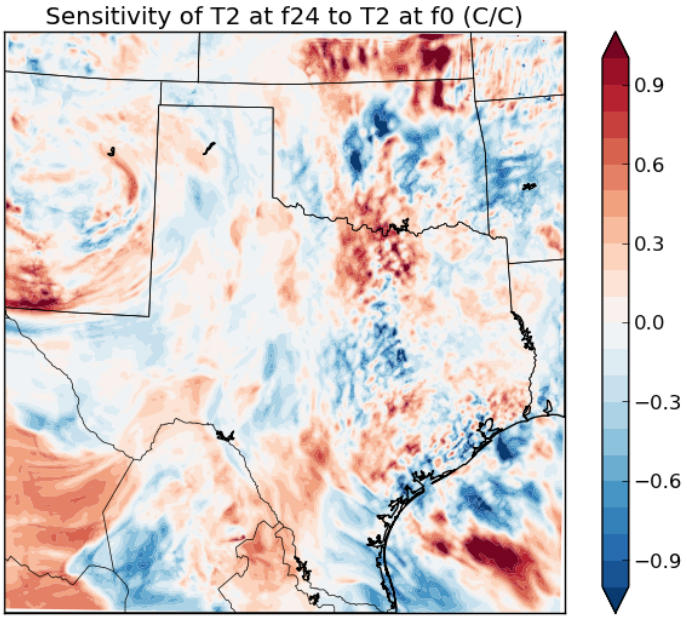

Figure 5: Ensemble sensitivity for three forecast metrics (a) max dBZ (dBZ deg C^{-1}), (b) max vertical velocity (m s^{-1} deg C^{-1}), and (c) average 2-meter temperature (deg C deg C^{-1}).

(a)

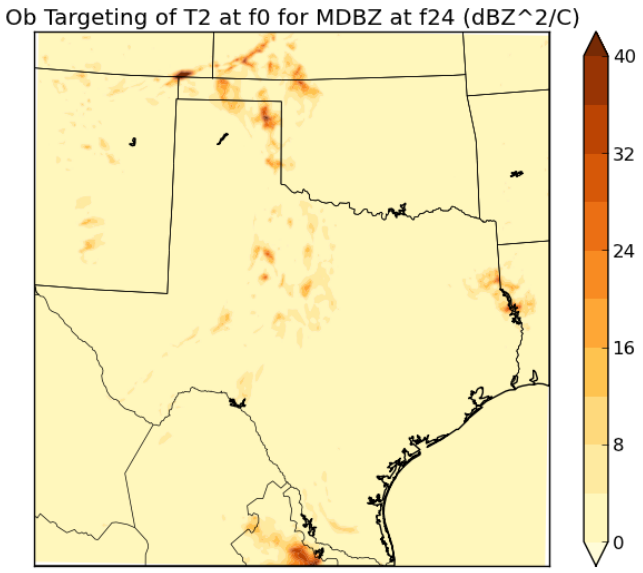
Ob Targeting of T2 at f0 for MDBZ at f24 (dBZ^2/C)
40
32
24
16
8
0

(b)

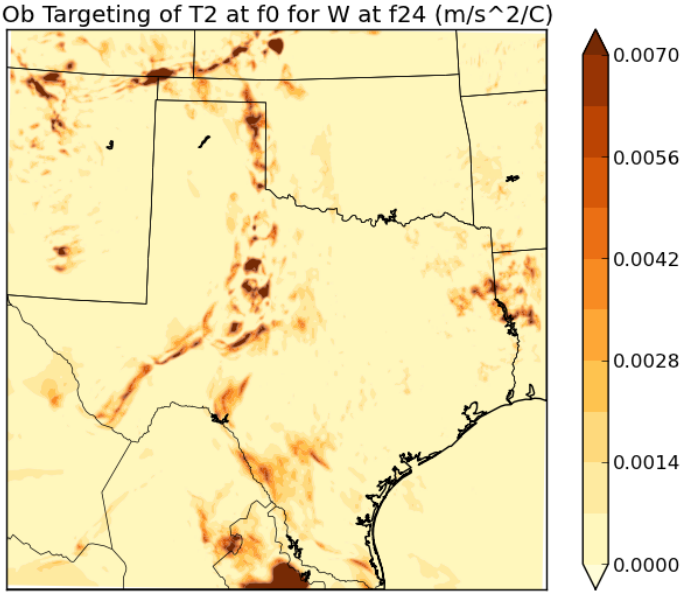
Ob Targeting of T2 at f0 for W at f24 (m/s^2/C)
0.0070
0.0056
0.0042
0.0028
0.0014
0.0000

(c)

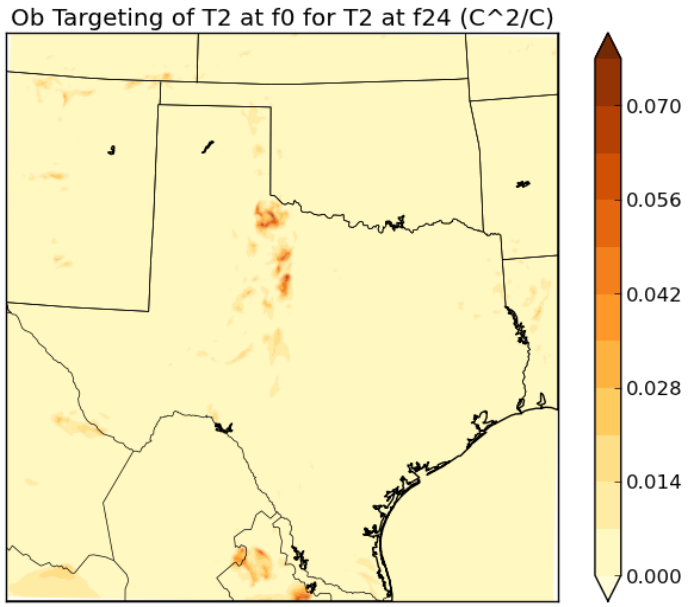

Figure 6: Observation targeting for three forecast metrics (a) max dBZ (dBZ^2 deg C^{-1}), (b) max vertical velocity (m^2 s^{-2} deg C^{-1}), and (c) average 2-meter temperature (deg C^2 deg C^{-1}).

(a)

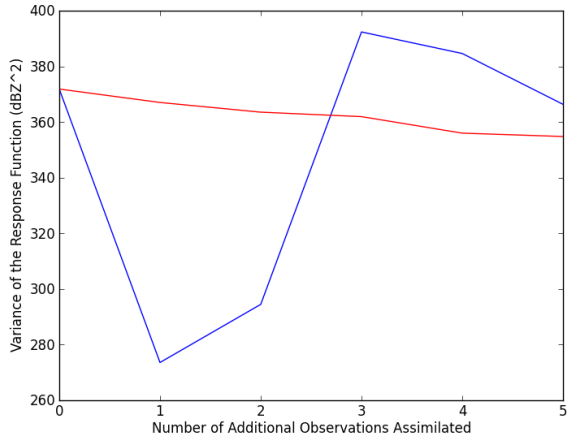

(b)

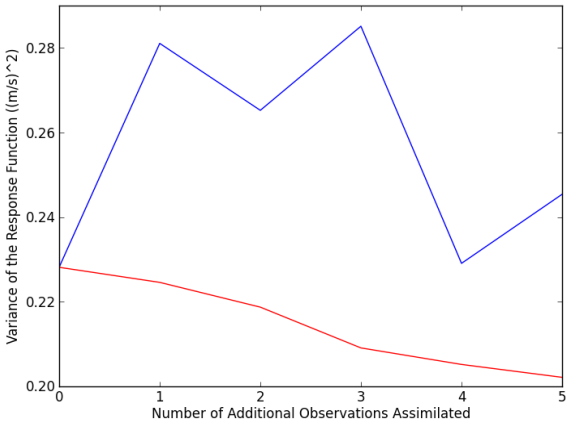

(c)

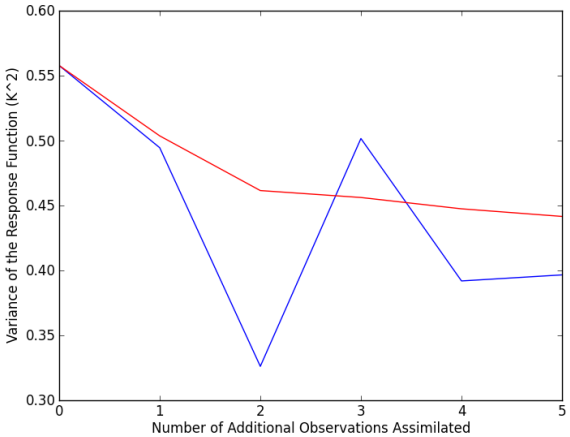

Figure 7: Expected (red) and actual (blue) variance of the forecast metrics (a) max dBZ (dBZ^2), (b) max vertical velocity ($m^2\ s^{-2}$), and (c) average 2-meter temperature (K^2) as additional observations are assimilated.